Electrochemistry Communications 127 (2021) 107038

Contents lists available at ScienceDirect

Electrochemistry Communications

journal homepage: www.elsevier.com/locate/elecom

Perovskite lead-based oxide anodes for rechargeable batteries

Anshuman Chaupatnaik, Prabeer Barpanda

Faraday Materials Laboratory (FaMaL), Materials Research Centre, Indian Institute of Science, Bangalore 560012, India

ARTICLE INFO

Keywords:
Battery
Anode materials
Perovskite
$PbTiO_3$

ABSTRACT

Lead-based perovskites ($PbTiO_3$ and $PbZrO_3$) are introduced as novel anode materials for non-aqueous M-ion rechargeable batteries (M = Li, Na, K). These compounds were scalably prepared by conventional solid-state (dry) and combustion (wet) routes. Charge storage in these perovskites involves a standard conversion ($Pb^{II} \rightarrow Pb^0$) followed by reversible Li-Pb/Na-Pb/K-Pb (de)alloying reaction. The oxide matrix (M_2O, TiO_2 etc.) phase is crucial for reversibility of Pb alloying reaction, as pristine PbO fails fast. The conversion-alloying reaction mechanism has been verified by ex situ electron microscopy (TEM) study. $PbTiO_3$ delivered 410 mAh/g capacity in the first charge vs. Li/Li^+ and Na/Na^+, while around 180 mAh/g capacity was observed vs. K/K^+. Particularly, $PbTiO_3$ forms a robust anode for sodium-ion batteries with maximum charge extracted under low voltage (below 0.8 V vs. Na/Na^+, 275 mAh/g). Similar electrochemical activity was also noticed for other perovskites like $PbZrO_3$ that confirms Pb-based (simple and mixed) perovskites can form a potential class of battery anode materials.

1. Introduction

The quest to '*build better batteries*' has unveiled many (post graphite) anode materials using (de)intercalation, conversion and (de)alloying reaction. Just 3 years after SONY®'s commercialization of the Li-ion battery (circa 1991), Miyasaka group reported an Sn-based amorphous tin composite oxide (ATCO) glass as a robust anode delivering four times volumetric and two times gravimetric energy density than graphite [1–3]. Based on this idea, a new company Fujifilm Celltec Co. Ltd. came up to develop and produce a new generation of lithium batteries named the STALION (aka Sn-based Li-Ion) cells and related products [4]. It triggered a wave of research activity over the next decade to study Sn-based compounds with alloying reaction. Some such materials are Sn-based borate-phosphate/ silicate glasses, spinels [5], hollandites [6] and $ASnX_3$ perovskite type phases with diverse A elements [7–12] storing lithium by a conversion-alloying reaction.

It is key to note the application of perovskites in energy storage. Perovskites (ABX_3) have oxygen (O) or halogen anions in the X positions at face center, small B cations at corners inside 6 fold O coordination (*Oct*ahedra cavity) and big A cations at body center inside 12 fold O coordination (*CubOct*ahedra) [13]. They are widely used in dielectric, ferroelectric, piezoelectric and photovoltaic applications. In addition to Sn-based perovskites (e.g. $CaSnO_3$), some studies exist on Ti-based perovskites. For example, $Li_{0.5}La_{0.5}TiO_3$ is a topotactic Li insertion anode (225 mAh/g) operating on the Ti redox [14,15], while $Na_{0.5}Bi_{0.5}TiO_3$ uses a soft Bi alloying center to store Na ions by conversion-alloying process [16]. Organic-inorganic lead halide (photovoltaic) perovskites $CH_3NH_3PbX_3$ (X = I, Cl, Br) can also store lithium ions involving framework breakdown-Pb alloying albeit with poor pristine structure stability [17]. Recently, various organic-inorganic and all-inorganic halide perovskite compounds have been reported as high capacity anode materials for (non)aqueous batteries [18–22].

On another note, like Sn, Pb alloying center can be exploited for charge storage. Pb alloying center was also tested in PbO:0.35 B_2O_3:0.35 P_2O_5 glass matrix similar to Fujifilm's ATCO glass [23], where aggregation rate and equilibrium cluster size were found larger for Pb than for Sn possibly due to Pb's softer polarizable nature. However, Pb containing simple perovskites have not been tested so far in secondary batteries. In the current work, we have combined the concepts of 'Pb alloying center' and 'perovskite framework' to present $PbTiO_3$ and $PbZrO_3$ perovskites as anodes in a march to set up perovskite $PbBX_3$ or $Pb(B'B'')X_3$ sub-class of battery anode materials. It marks the first report on usage of simple Pb-based perovskites to reversible store charge from alloying reactions of Pb with Li, Na or K that can store upto 4.4 Li ($Li_{22}Pb_5$, 568 mAh/g), 3.75 Na ($Na_{15}Pb_4$, 485 mAh/g) or 1 K (KPb, 129 mAh/g) per Pb atom, while only 1 Li/K can be held by 6C (LiC_6, 372 mAh/g) or 8C (KC_8, 279 mAh/g) atoms. Further graphite anode cannot intercalate Na ions preventing it's use in sodium-ion batteries, while a large amount of Na (as high as 406 mAh/g, 4.6 Na/$PbTiO_3$) can be stored in the perovskite $PbTiO_3$. These low-voltage, high-capacity

E-mail address: prabeer@iisc.ac.in (P. Barpanda).

https://doi.org/10.1016/j.elecom.2021.107038
Received 19 February 2021; Received in revised form 7 April 2021; Accepted 7 April 2021
Available online 15 April 2021

perovskite anodes ($PbTiO_3$ and $PbZrO_3$) can be scalably prepared and are extreme stable under ambient conditions unlike its organic-inorganic lead halide counterparts or non-perovskite PX-$PbTiO_3$ phases. Besides, these phases are weatherproof, and non-toxic than pristine lead metal or lead oxides. This report paves the way for usage of all lead-based compounds with simple perovskite ABX_3 and their derivative frameworks as anodes for high energy density rechargeable batteries.

2. Material and methods

Lead titanate ($PbTiO_3$), and lead zirconate ($PbZrO_3$) were prepared by conventional solid-state (dry) and solution combustion (wet) methods. The respective oxides (Litharge PbO, SDFine, 98%; TiO_2, Merck, 99%; and ZrO_2, Merck, 99%) were hand mixed, pelletized, and calcined at 600° or 900 °C for 24 h (in air) with intermediate grinding after 12 h. Combustion synthesis was carried out using nitrate oxidizers (O) ($Pb(NO_3)_2$, SDFine, 99.5%; in-house prepared $TiO(NO_3)_2$ [24]), and glycine fuel (F) ($C_2H_5NO_2$, Merck, 99.7%) in 1:1 O/F ratio over an ice bath. The intermediate product was pelletized and calcined at 400 °C for 2 h (in air). Phase identification was performed using a Cu Kα X-ray source (λ = 1.54 Å) with a Bruker D8 Discover X-ray diffractometer (operating at 40 kV/35 mA). Rietveld refinement [25] was performed using the GSAS software [26]. The powder samples were dispersed in isopropyl alcohol (C_3H_8O, Merck, ≥99.5%), sonicated for 10 min and drop cast onto carbon film mesh copper grids (EMS). They were used for transmission electron microscopy (TEM) employing an FEI Tecnai T20ST microscope operating at 200 kV.

Active material, Super P carbon black (Alfa Aesar, 99+%), and Sodium CarboxyMethyl Cellulose salt (Sigma) (CMC) were taken in an 80:10:10 ratio (100 mg total dry weight per batch), hand mixed after adding distilled water (500 μl per batch) to form grey electrode ink that was dropcast on precut SS304 or battery grade Cu foil. After drying at 60 °C to remove water, the electrodes were dried under vacuum at 120 °C (Büchi Glass Oven B-585) overnight and transferred into Ar-filled glovebox (MBraun LabStar GmbH, O_2 and H_2O levels <0.5 ppm). The coatings were used against respective M (Li/Na/K) metal foils as counter electrodes to assemble CR2032 type coin cells or half-inch SS304 Swagelok cells. 1 M $LiPF_6$ dissolved in 1:1:3 v/v % of ethylene carbonate/propylene carbonate/dimethyl carbonate (EC/PC/DMC) was used as the lithium electrolyte (Chameleon Reagent). 1 M $NaPF_6$ or 0.5 M KPF_6 dissolved in 0.45:0.45:0.1 v/v% EC/PC/DMC was used as electrolytes in sodium and potassium ion batteries. The current given was one Faraday charge, per unit mole of active material in 20 h (C/20, i.e. 4.4 mA/g and 3.87 mA/g for $PbTiO_3$ and $PbZrO_3$ respectively). Cells were cycled with a Neware BTS4000 battery tester in a voltage window of 0.01 V to upper cut off (0.8, 2, 2.5 or 3 V), without any rest time in between charge and discharge.

For ex situ analysis, cycled swageloks were disassembled inside glovebox and the recuperated electrodes were washed using Dimethyl Carbonate (DMC, anhydrous, ≥99%). Electrode materials, scratched from the washed electrode, was dispersed in anhydrous DMC. It was drop cast on TEM grids inside the glovebox and dried overnight in Büchi B-585 glass oven before examination.

3. Results and discussion

Phase-pure $PbTiO_3$ was obtained via combustion synthesis (as well as solid-state route). TEM micrograph indicates the formation of sub-micron particle size (Fig. 1a). HRTEM shows (0 0 1) planes with an interplanar spacing of 4.06 Å (Fig. 1b). SAED pattern was indexed to zone axis [−1 3 3] (Fig. 1c) confirming the crystallinity of desired product. Rietveld refinement of powder XRD pattern was performed using GSAS software (Fig. 1d) [26]. It confirmed the formation of tetragonal (s.g. *P4mm*, #99) framework with lattice parameters: $a = b =$ 3.9027(6) Å, c = 4.1404(6) Å along with acceptable goodness of fit (Table S1). Single-phase $PbTiO_3$ and $PbZrO_3$ end-members were also

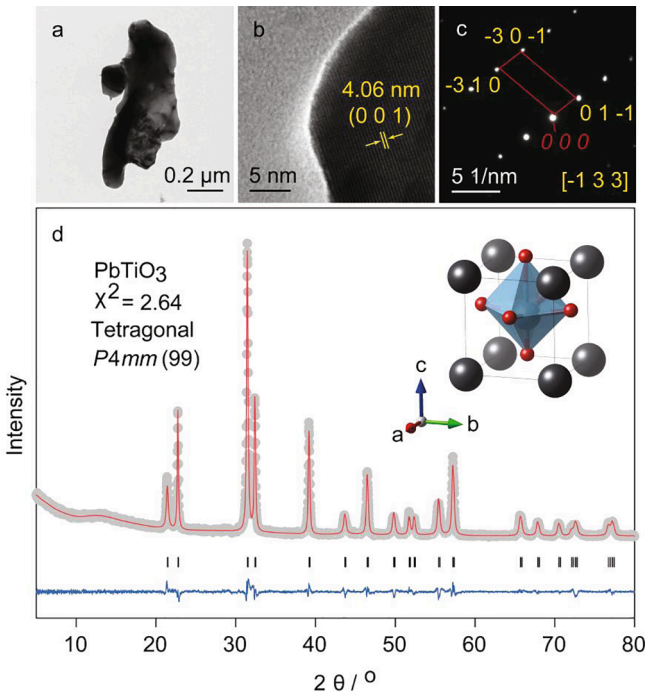

Fig. 1. (a) Representative bright field TEM micrograph, (b) HRTEM image, (c) SAED pattern, and (d) Rietveld refinement of XRD (Cu K_α) pattern of $PbTiO_3$ synthesized by solution combustion route (400 °C, 2 h). Experimental data points (grey filled circles), calculated pattern (red line), their difference (blue line), and Bragg reflections (black sticks) of tetragonal *P4mm* phase are shown in (d), inset shows the crystal structure (Pb = black balls, O = red balls, TiO_6 = distorted blue octahedra). (For interpretation of the references to colour in this figure legend, the reader is referred to the web version of this article.)

obtained via solid-state synthesis. Unlike $PbTiO_3$, perovskite $PbZrO_3$ assumed an orthorhombic (s.g. *Pbam*, #55) crystal structure (Table S2, Fig. S1).

The combustion synthesized $PbTiO_3$ was tested in lithium half-cell architecture. Fig. 2 depicts the respective electrochemical performance. The redox mechanism follows two-steps.

First – irreversible conversion step [$PbTiO_3 + 2\ Li^+ + 2e^- \rightarrow Pb + TiO_2 + Li_2O$]: Here, two electrons are used (Pb^{2+} to Pb^0) as the parent structure breaks down slowly into constituent alloying element(s) (here, Pb) and Li_2O. Oxides of any spectator non-alloying element (here, TiO_2) are formed, which like Li_2O, are preferred over elemental form due to high bond strength with oxygen [7]. *In-situ* formation of TiO_2 matrix was confirmed from diffuse rings in the SAED pattern (Fig. S6b) of a partly discharged region at 0.5 V with $PbTiO_3$ (spots) as major phase (Fig. S6a). The growth of new phases generates a flat two-phase voltage plateau at a value related to the stability of the parent structure (Fig. 2a). Here, it occurs at 0.74 V compared to the 1.4 V flat profile for PbO, which indicates the PbO framework is more stable than the $PbTiO_3$ structure (Fig. 2c). After structure breakdown (via conversion), Pb or Li_xPb cubes were obtained with different morphology from starting $PbTiO_3$ phase (Fig. 2a inset). Absence of the 0.74 V discharge peak in following cycles rules out the reformation of $PbTiO_3$ at the end of charge (Fig. 2c). Upon formation, the Pb particles aggregate and are electrochemically active as evidenced by sharp dQ/mdV peaks (Fig. 2c). These Pb aggregates reach a critical size either after the conversion reaction or after few (de) alloying reactions. Some extra capacity can arise due to electrolyte reduction during the conversion reaction. Similar observations were reported for Sn-based anodes [7,27].

Second – reversible (de)alloying step [$Pb + xLi^+ + xe^- \leftrightarrow Li_xPb$ ($x \leq 4.4$)]: Gradual alloying reaction occurs involving Pb reversibly storing Li in forms of intermetallic compounds that may (not) follow the

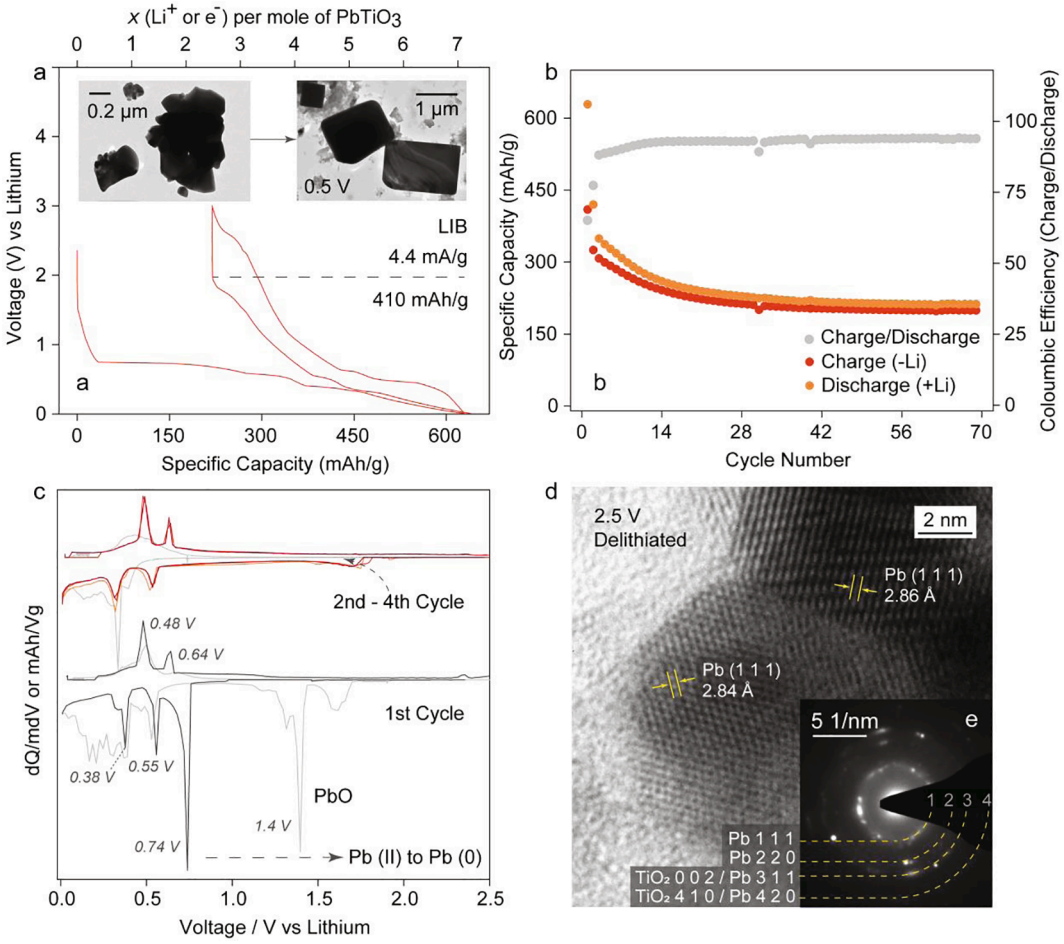

Fig. 2. Electrochemical performance of combustion synthesized $PbTiO_3$ vs lithium. (a) Voltage capacity plot, (b) capacity fade, (c) differential capacity curve (dQ/mdV) of first two cycles (PbO curves greyed), (d) HRTEM micrograph, and (e) SAED pattern of ex situ samples after 1st charge at 2.5 V showing Pb particle. (*Inset* of a) Left inset shows pristine particle and right inset illustrates Pb or Li_xPb cubes after 1st discharge to 0.5 V.

equilibrium phase diagram. Two intermediate phases, most likely LiPb and $Li_{2.6}Pb$, form reversibly as indicated from pairs of 0.55 V/0.64 V and 0.38 V/0.48 V peaks (Fig. 2c) [28]. $Li_{4.4}Pb$ forms at the end of first discharge as confirmed by ~4.4 electron insertion after 2 electron for $Pb^{II} \rightarrow Pb^0$ reduction (Fig. 2a).

Here, the matrix TiO_2 phase may also partially participate in reversible Li storage (forming Li_xTiO_2). The Pb dealloying from $Li_{4.4}Pb$ and Li de-insertion from Li_xTiO_2 results in a first charge capacity of 410 mAh/g, fading to 200 mAh/g after 70 cycles, when cycled at low 4.4 mA/g current (Fig. 2b). The charge capacity is around 120 mAh/g at very high 352 mA/g current, corresponding to 4 Li insertion in an hour (Fig. S2). The reversible first charge capacity was 184 mAh/g for restricted 0.8 V window (Fig. S3). Pb particles embedded in amorphous TiO_2 matrix can be clearly seen at the end of this 1st charge/dealloying reaction (Fig. 2d, e). The matrix phase is critical to reversibility of the (de)alloying reaction. Without a well-developed matrix, PbO cannot handle the volume changes occuring as early as the second cycle itself (Fig. 2c) and fails completely within few cycles (Fig. S5a). Co-existence of two phases (the second step) with different volumes have been reported to lead to microcrack, electrode delamination and capacity fade. Inactive Li_2O oxide matrix generated *in-situ* during first step pins alloying element (Fig. S7a and b), restricts massive aggregation and provides an elastic-cushion for checking large volume expansion typical for alloying reactions. It is reported that despite capacity loss, more spectator ions lead to fewer aggregation of alloying element and restricted volume change favoring less delamination and better capacity retention [27].

Inspired by the success in Li-half cell and possibility of Pb alloying with Na/K metals, $PbTiO_3$ perovskite was tested for post-Li-ion (Na-ion/K-ion) batteries (Fig. 3). In both cases, merger of conversion and alloying steps was noticed. In addition to Na/K metals' low voltage (w.r.t. Li), this merger could stem from Pb's strong alloying tendency at its respective voltage driving the onset of initial conversion (and framework rupture). In sodium half-cell, there are two plateaus during discharge (total 7.5 electrons): one at 0.17 V likely from conversion reaction involving framework collapse and another at 0.03 V due to alloying reaction (Fig. 3c). During the first charge, four peaks indicate sequential dealloying involving $Na_{15}Pb_4$ (0.18 V) → Na_9Pb_4/Na_5Pb_2 (0.24 V) → NaPb (0.44 V) → $NaPb_3$ (0.55 V) [29]. A small capacity arises near 1.5 V in the initial cycles, which could arise from Na (de)insertion in TiO_2 matrix. The capacity fade upon cycling can be due to damage of TiO_2 by Na insertion, or the coarsening of Pb particles due to (de)alloying that further mutilates TiO_2 affecting its Na insertion capability. The matrix ensures reversibility during (de)alloying, which fail in PbO in few cycles (Fig. S5b).

In sodium half-cell, reversible first charge capacity was 406 mAh/g for full window (ca. 2.5 V) and 275 mAh/g for restricted window (ca. 0.8 V). It highlights another important incentive for using $PbTiO_3$ as NIB anode (vis-à-vis as LIB anode): a large part of the charge capacity (275 mAh/g) occurs below 0.8 V (vs. Na), which is significantly higher than the capacity (184 mAh/g) vs. Li. This is due to lower standard reduction potential of Na compared to Li. The dearth of non-carbonaceous anode materials for sodium-ion batteries makes perovskite $PbTiO_3$ a promising high-capacity anode with low voltage operation.

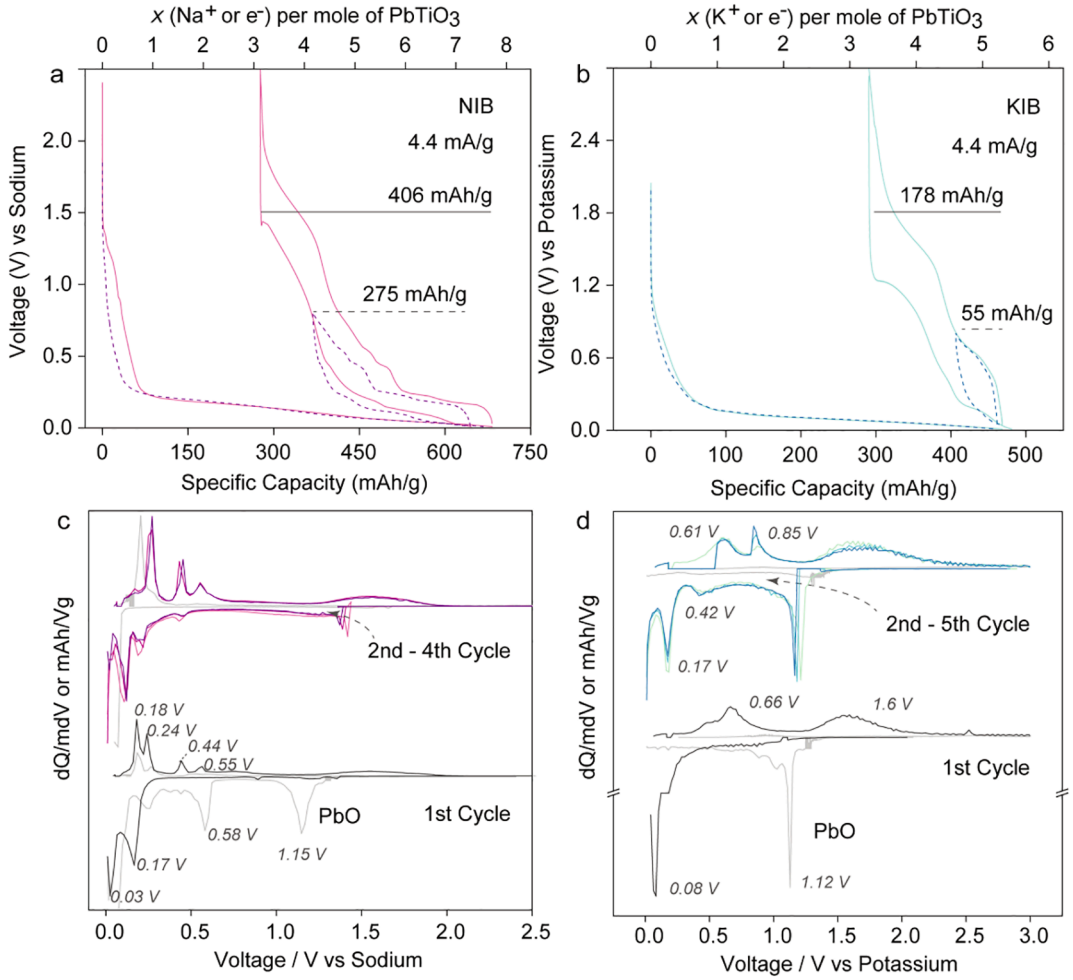

Fig. 3. Electrochemical performance of combustion synthesized $PbTiO_3$ vs sodium and potassium. (a, b) Voltage capacity, and (c, d) differential capacity plots for the first two cycles (PbO profiles greyed).

When $PbTiO_3$ was tested in K-half cell, only one reduction plateau was observed ~0.08 V yielding a first discharge capacity of 450 mAh/g (or 5 electrons) (Fig. 3b). It involves overlapping of conversion and alloying reaction step. Upon cycling, new peaks evolve below 0.8 V owing to formation of K_xPb phases (Fig. 3d) such as $K_{10}Pb_{48}$ (~0.42 V) and K_4Pb_9 (~0.6 V) [30]. At later cycles, the sharp discharge peak ~1.16 V may stem from electrolyte reaction with Pb metal or reversible K-TiO_2 insertion. These events add to higher reversible capacity (first charge) of around 178 mAh/g in the wide potential window up to 3 V, while a meagre 55 mAh/g capacity is observed below 0.8 V (Fig. 3b). Unlike the Li and Na case, perovskite $PbTiO_3$ was found to have poor activity for K-ion batteries.

Simple Pb-based perovskites work as anodes for secondary Li-ion and Na-ion batteries based on conversion-alloying reaction. In this context, few points can be highlighted.

(1) The net electrochemical activity is dependent on particle size and hence the synthesis route. Owing to Ostwald ripening and grain growth, solid-state synthesis led to larger micrometric (2–4 μm) particles vis-à-vis sub-micron (0.2–0.8 μm) particles obtained by wet combustion route. For example, the solid-state made $PbTiO_3$ delivered less capacity (368 mAh/g) than combustion prepared $PbTiO_3$ (410 mAh/g) due to larger particle size hindering the initial conversion reaction. Finer microstructure of starting perovskite is preferred for superior activity.

(2) The concept of Pb-based perovskite anode can be extended to redox inactive transition metal-based counterparts. To illustrate this point, solid-state made $PbZrO_3$ perovskite was tested in Li- and Na-half cells (Fig. 4). It delivered reversible electrochemical activity involving alloying reactions following initial conversion reaction. As expected, due to higher molecular weight, $PbZrO_3$ yielded lower capacity (291 mAh/g) in comparison to $PbTiO_3$ (368 mAh/g) (Fig. 4a, c). The initial conversion reaction for $PbTiO_3$ occurs at 56 mV higher than $PbZrO_3$ indicating higher stability of $PbTiO_3$.

(3) Other Pb-based perovskites (e.g. $PbZrO_3$) can be employed in sodium-ion batteries as well. $PbZrO_3$ delivered a reversible capacity of 65 mAh/g (Fig. 4b, d) involving multiple (de)alloying steps. Two things can be concluded from changing Ti to Zr. One, the alloy stabilization is delayed over few cycles due to heavier Zr (Fig. S4). Second, in case of $PbZrO_3$, capacity around 1.5 V is significantly reduced (for both Li and Na). Thus, the small activity ~1.5 V can be assigned to Ti redox in $PbTiO_3$ for all alkali insertion.

(4) Although toxic, with careful handling, Pb-based compounds have been extensively used as lead-acid accumulators in automobiles and inverters. Pb-acid batteries offer an excellent recycling efficiency as high as 99%. Both in elemental form or as oxides, the alloying reaction of Pb with Li, Na and K is well established. Metallic lead (Pb) and its volatile oxides (e.g. PbO) can be unsafe. This safety concern can be mitigated by embedding Pb in perovskite structure, which works as a reservoir for Pb metal ions for use in (de)alloying reaction based rechargeable batteries.

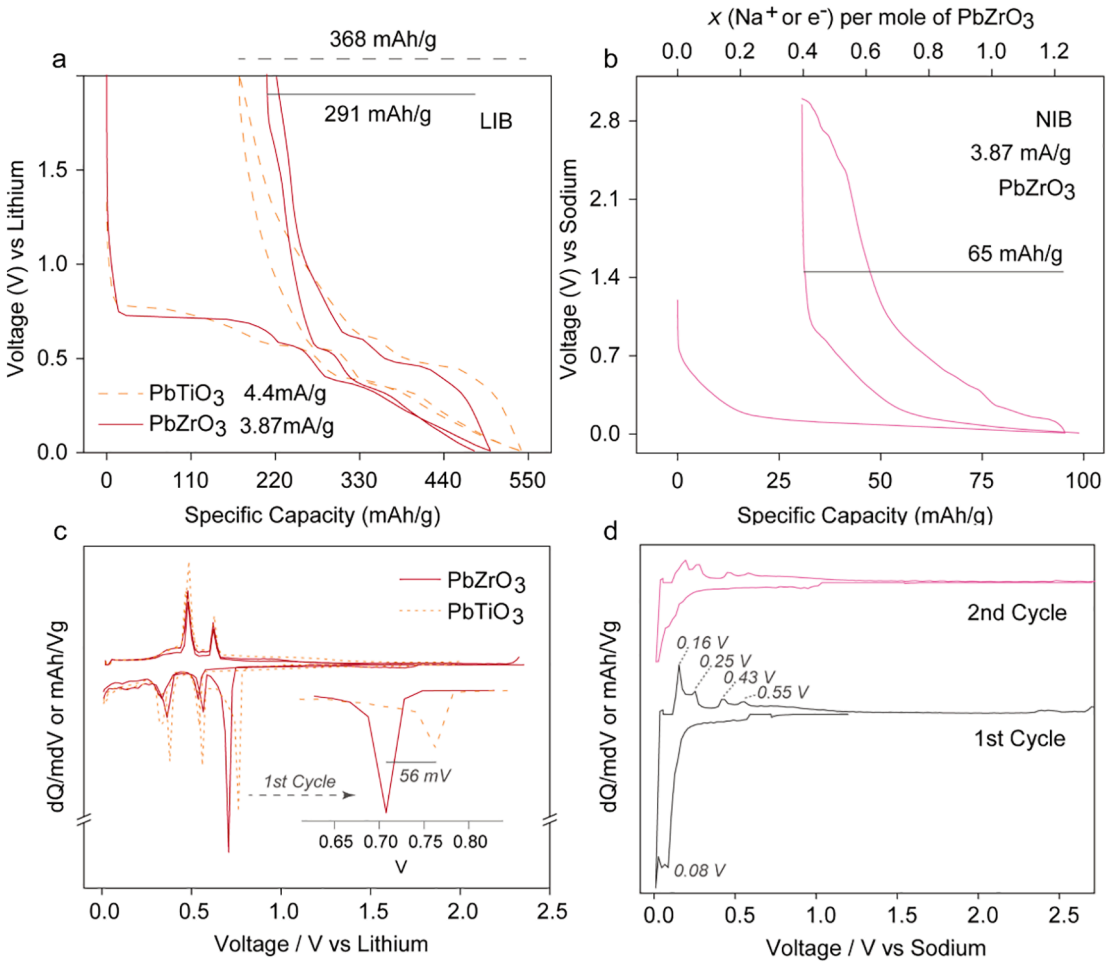

Fig. 4. Electrochemical performance of $PbTiO_3$ and $PbZrO_3$ made by solid-state method: (a) Voltage-capacity plot, and (c) Differential capacity plot versus lithium. (b) Voltage capacity plot, and (d) differential capacity plot of first two cycles versus sodium.

Thus, we propose oxide perovskites as safe lead-based compounds capable of Pb-alloying reaction to yield high voltage, high energy density non-aqueous Li-ion or Na-ion batteries. While they are promising, it warrants future investigation to unveil (a) the detail electrochemical reaction mechanism involving *operando* X-ray diffraction, (b) probing the reaction products (Pb, TiO_2, Li_xPb, Li_2O) and their distribution at various states of (dis)charge using high-resolution electron microscopy, and (c) calculating the reaction energetics using first-principle (DFT) calculations.

4. Conclusions

Lead-based perovskites, $PbTiO_3$ and $PbZrO_3$, prepared by solid-state (dry) and solution combustion (wet) routes, have been introduced as anodes for variety of alkali-ion (M = Li, Na, K) batteries. First, the parent perovskite materials undergo irreversible conversion to Pb, M_2O and other oxides at a voltage depending on stability of the parent material. Next, in the inactive oxide matrix, Pb undertakes reversible (de)alloying with M forming multiple intermediate line compounds (or alloys) as per Pb–M phase diagrams. The end phases formed at the end of first discharge are most likely $Li_{4.4}Pb$, $Na_{3.75}Pb$ and K_1Pb based on number of M inserted per mole of starting material. Perovskite $PbTiO_3$ yielded a reversible (1st charge) capacity of 410 mAh/g (for Li/Na-half cell) and 180 mAh/g (for K-half cell). Highest reversible capacity under 0.8 V was observed in Na-half cell, making $PbTiO_3$ a promising anode for sodium batteries. Pb-based perovskites offer a safe repository of anodes involving Pb (de)alloying reaction. These simple perovskites and their derivatives can realize high energy density batteries [31]. It can open door to design suites of Pb-based perovskite anodes armed with scalable synthesis, chemical/thermal stability, high energy density, safe handling/usage and easy recycling.

CRediT authorship contribution statement

Anshuman Chaupatnaik: Conceptualization, Methodology, Investigation, Data curation, Writing - original draft. **Prabeer Barpanda:** Supervision, Writing - review & editing, Project administration, Funding acquisition.

Declaration of Competing Interest

The authors declare that they have no known competing financial interests or personal relationships that could have appeared to influence the work reported in this paper.

Acknowledgements

We acknowledge the financial support from the Technology Mission Division (Department of Science and Technology, Government of India) under the aegis of Materials for Energy Storage (MES-2018) program (DST/TMD/MES/2K18/00217). A.C.P. thanks the Advanced Facility for Microscopy and Microanalysis (AFMM, IISc) for access to TEM facility.

Appendix A. Supplementary data

Supplementary data to this article can be found online at https://doi.org/10.1016/j.elecom.2021.107038.

References

[1] Y. Idota, M. Mishima, Y. Miyaki, T. Kubota, T. Miyasaka, U.S. Patent 5,618,640A (1994), https://patents.google.com/patent/US5618640A/en.

[2] Y. Idota, T. Kubota, A. Matsufuji, Y. Maekawa, T. Miyasaka, Tin-based amorphous oxide: a high-capacity lithium-ion-storage material, Science 276 (1997) 1395–1397, https://doi.org/10.1126/science.276.5317.1395.

[3] R.A. Huggins, Lithium alloy negative electrodes formed from convertible oxides, Solid State Ionics 113–115 (1998) 57–67, https://doi.org/10.1016/s0167-2738(98)00275-6.

[4] I.A. Courtney, J.R. Dahn, Electrochemical and in situ X-ray diffraction studies of the reaction of lithium with tin oxide composites, J. Electrochem. Soc. 144 (1997) 2045–2052, https://doi.org/10.1149/1.1837740.

[5] P.A. Connor, J.T.S. Irvine, Novel tin oxide spinel-based anodes for Li-ion batteries, J. Power Sources 97–98 (2001) 223–225, https://doi.org/10.1016/S0378-7753(01)00545-6.

[6] N. Sharma, J. Plévert, G.V. Subba Rao, B.V.R. Chowdari, T.J. White, Tin oxides with hollandite structure as anodes for lithium ion batteries, Chem. Mater. 17 (2005) 4700–4710, https://doi.org/10.1021/cm0505042.

[7] N. Sharma, K.M. Shaju, G.V. Subba Rao, B.V.R. Chowdari, Sol-gel derived nano-crystalline $CaSnO_3$ as high capacity anode material for Li-ion batteries, Electrochem. Commun. 4 (2002) 947–952, https://doi.org/10.1016/S1388-2481(02)00495-2.

[8] Y. Sharma, N. Sharma, G.V. Subba Rao, B.V.R. Chowdari, Lithium-storage and cycleability of nano-$CdSnO_3$ as an anode material for lithium-ion batteries, J. Power Sources 192 (2009) 627–635, https://doi.org/10.1016/j.jpowsour.2009.02.096.

[9] X. Li, C. Wang, Significantly increased cycling performance of novel "self- matrix" $NiSnO_3$ anode in lithium ion battery application, RSC Adv. 2 (2012) 6150–6154, https://doi.org/10.1039/c2ra20527k.

[10] Y. Chen, B. Qu, L. Mei, D. Lei, L. Chen, Q. Li, T. Wang, Synthesis of $ZnSnO_3$ mesocrystals from regular cube-like to sheet-like structures and their comparative electrochemical properties in Li-ion batteries, J. Mater. Chem. 22 (2012) 25373–25379, https://doi.org/10.1039/c2jm33123c.

[11] Z. Wang, Z. Wang, W. Liu, W. Xiao, X.W. Lou, Amorphous $CoSnO_3$@C nanoboxes with superior lithium storage capability, Energy Environ. Sci. 6 (2013) 87–91, https://doi.org/10.1039/C2EE23330D.

[12] P. Nithyadharseni, M.V. Reddy, K.I. Ozoemena, F.I. Ezema, R.G. Balakrishna, B.V. R. Chowdari, Electrochemical performance of $BaSnO_3$ anode material for lithium-ion battery prepared by molten salt method, J. Electrochem. Soc. 163 (2016) A540–A545, https://doi.org/10.1149/2.0961603jes.

[13] D.W. Murphy, P.A. Christian, Solid state electrodes for high energy batteries, Science 205 (1979) 651–656, https://doi.org/10.1126/science:205.4407.651.

[14] C. Hua, X. Fang, Z. Wang, L. Chen, Lithium storage in perovskite lithium lanthanum titanate, Electrochem. Commun. 32 (2013) 5–8, https://doi.org/10.1016/j.elecom.2013.03.038.

[15] L. Zhang, X. Zhang, G. Tian, Q. Zhang, M. Knapp, H. Ehrenberg, G. Chen, Z. Shen, G. Yang, L. Gu, F. Du, Lithium lanthanum titanate perovskite as an anode for lithium ion batteries, Nat. Commun. 11 (2020) 1–8, https://doi.org/10.1038/s41467-020-17233-1.

[16] K.K. Bharathi, B. Moorthy, H.K. Dara, L. Durai, D.K. Kim, Electrochemical properties of $Na_{0.5}Bi_{0.5}TiO_3$ perovskite as an anode material for sodium ion batteries, J. Mater. Sci. 54 (2019) 13236–13246, https://doi.org/10.1007/s10853-019-03834-9.

[17] H.R. Xia, W.T. Sun, L.M. Peng, Hydrothermal synthesis of organometal halide perovskites for Li-ion batteries, Chem. Commun. 51 (2015) 13787–13790, https://doi.org/10.1039/C5CC05053G.

[18] L. Zhang, J. Miao, J. Li, Q. Li, Halide perovskite materials for energy storage applications, Adv. Funct. Mater. 30 (2020) 2003653, https://doi.org/10.1002/adfm.202003653.

[19] A. Kostopoulou, D. Vernardou, D. Makri, K. Brintakis, K. Savva, E. Stratakis, Highly stable metal halide perovskite microcube anodes for lithium-air batteries, J. Power Sources Adv. 3 (2020) 100015, https://doi.org/10.1016/j.powera.2020.100015.

[20] N. Vicente, D. Bresser, S. Passerini, G. Garcia-Belmonte, Probing the 3-step lithium storage mechanism in CH_3NH_3PbBr 3 perovskite electrode by *Operando*-XRD analysis, ChemElectroChem 6 (2019) 456–460, https://doi.org/10.1002/celc.201801291.

[21] D. Ramirez, Y. Suto, N.C. Rosero-Navarro, A. Miura, K. Tadanaga, F. Jaramillo, Structural and electrochemical evaluation of three- and two-dimensional organohalide perovskites and their influence on the reversibility of lithium intercalation, Inorg. Chem. 57 (2018) 4181–4188, https://doi.org/10.1021/acs.inorgchem.8b00397.

[22] J.A. Dawson, A.J. Naylor, C. Eames, M. Roberts, W. Zhang, H.J. Snaith, P.G. Bruce, M.S. Islam, Mechanism of lithium intercalation and conversion processes in organic-inorganic halide perovskites, ACS Energy Lett. 2 (2017) 1818–1824, https://doi.org/10.1021/acsenergylett.7b00437.

[23] I.A. Courtney, W.R. McKinnon, J.R. Dahn, On the Aggregation of tin in SnO composite glasses caused by the reversible reaction with lithium, J. Electrochem. Soc. 146 (1999) 59–68, https://doi.org/10.1149/1.1391565.

[24] A. Chaupatnaik, P. Barpanda, Swift combustion synthesis of $PbLi_2Ti_6O_{14}$ anode for lithium-ion batteries: diffusional and electrochemical investigation, J. Electrochem. Soc. 166 (2019) A5122–A5130, https://doi.org/10.1149/2.0191903jes.

[25] H.M. Rietveld, A profile refinement method for nuclear and magnetic structures, J. Appl. Crystallogr. 2 (1969) 65–71, https://doi.org/10.1107/s0021889869006558.

[26] B.H. Toby, R.B. Von Dreele, GSAS-II: the genesis of a modern open-source all purpose crystallography software package, J. Appl. Crystallogr. 2 (2013) 544–549, https://doi.org/10.1107/S0021889813003531.

[27] I.A. Courtney, J.R. Dahn, Key factors controlling the reversibility of the reaction of lithium with SnO_2 and Sn_2BPO_6 Glass, J. Electrochem. Soc. 144 (1997) 2943–2948, https://doi.org/10.1149/1.1837941.

[28] M. Martos, J. Morales, L. Sánchez, Lead-based systems as suitable anode materials for Li-ion batteries, Electrochim. Acta 48 (2003) 614–621, https://doi.org/10.1016/S0013-4686(02)00730-2.

[29] A. Darwiche, R. Dugas, B. Fraisse, L. Monconduit, Reinstating lead for high-loaded efficient negative electrode for rechargeable sodium-ion battery, J. Power Sources 304 (2016) 1–8, https://doi.org/10.1016/j.jpowsour.2015.10.087.

[30] V. Gabaudan, R. Berthelot, L. Stievano, L. Monconduit, Electrochemical alloying of lead in potassium-ion batteries, ACS Omega 3 (2018) 12195–12200, https://doi.org/10.1021/acsomega.8b01369.

[31] A. Chaupatnaik, P. Barpanda, Indian Patent Application # 202141004920.